

Energy-Efficient Multi-LLM Reasoning for Binary-Free Zero-Day Detection in IoT Firmware

Saeid Jamshidi, Omar Abdul-Wahab, Martine Bellaïche, and Foutse Khomh

Abstract—Securing Internet of Things (IoT) firmware remains difficult due to proprietary binaries, stripped symbols, heterogeneous architectures, and limited access to executable code. Existing analysis methods, such as static analysis, symbolic execution, and fuzzing, depend on binary visibility and functional emulation, making them unreliable when firmware is encrypted or inaccessible. To address this limitation, we propose a binary-free, architecture-agnostic solution that estimates the likelihood of conceptual zero-day vulnerabilities using only high-level descriptors. The approach integrates a tri-LLM reasoning architecture combining a LLaMA-based configuration interpreter, a DeepSeek-based structural abstraction analyzer, and a GPT-4o semantic fusion model. The solution also incorporates LLM computational signatures, including latency patterns, uncertainty markers, and reasoning depth indicators, as well as an energy-aware symbolic load model, to enhance interpretability and operational feasibility. In addition, we formally derive the mathematical foundations of the reasoning pipeline, establishing monotonicity, divergence, and energy-risk coupling properties that theoretically justify the model's behavior. Simulation-based evaluation reveals that high exposure conditions increase the predicted zero-day likelihood by 20–35% across models, with GPT-4o demonstrating the strongest cross-layer correlations and the highest sensitivity. Energy and divergence metrics significantly predict elevated risk ($p < 0.01$), reinforcing the effectiveness of the proposed reasoning framework.

Index Terms—IoT security, firmware analysis, zero-day vulnerabilities, large language models (LLMs), semantic reasoning, binary-free analysis, energy-aware computation.

I. INTRODUCTION

The security of Internet of Things (IoT) firmware has become a critical priority as billions of embedded devices operate autonomously in sensitive, remote, and unmonitored environments [1][2][3]. Firmware controls the most privileged layers of these devices, including hardware access, authentication mechanisms, protocol handling, and system initialization, making it a single point of failure for overall device integrity [4][5][6]. A single unnoticed flaw can grant adversaries persistent footholds, enable large-scale botnet deployment, disrupt industrial processes, and facilitate stealthy lateral movement across interconnected infrastructures [7][8]. As IoT ecosystems continue to expand in heterogeneity and complexity, ensuring firmware security has become essential to global cyber resilience [9][10].

Despite its importance, firmware analysis remains exceptionally difficult in practice [5][11]. IoT vendors frequently

employ encrypted binaries, proprietary compression formats, stripped symbols, and undocumented architectures, which render classical analysis, such as disassembly, symbolic execution, fuzzing, and sandboxing, often infeasible [12][13]. Many devices lack reliable update mechanisms, leaving long-lived vulnerabilities that are widely deployed. Firmware diversity across vendors and architectures complicates automated tooling, while anti-analysis defenses further restrict access to internal execution semantics [14]. As a result, existing techniques struggle to identify deeply embedded or previously unknown weaknesses, especially zero-day vulnerabilities that manifest conceptually rather than through known signatures [15].

In this challenging landscape, Large Language Models (LLMs) introduce a fundamentally new opportunity. In contrast to conventional tools that rely strictly on byte-level visibility, LLMs excel at semantic reasoning, hierarchical abstraction, and interpreting incomplete and high-level descriptions [16][17][18]. By analyzing metadata, configuration semantics, privilege structures, protocol roles, and lightweight opcode-shape descriptors, LLMs can infer structural inconsistencies and dangerous patterns suggestive of conceptual zero-day risks, even without access to the raw firmware binary [19]. Their capacity for generalization, cross-layer correlation, and multi-view reasoning enables security assessments in scenarios where binary access is restricted and entirely unavailable.

Although researchers' efforts have advanced IoT firmware security, limitations persist. ArgXtract [20] extracts configuration artifacts from stripped binaries, while HermesScan [21] accelerates static vulnerability detection through enhanced reaching-definition analysis. Directed fuzzing frameworks [22] uncover memory-safety weaknesses but require accurate emulation environments. Taint-based analyzers [23] track unsafe data propagation yet depend on symbolic visibility. Field studies [24] document vulnerabilities in deployed systems, and network-based botnet detection approaches [25] identify malicious behaviors but provide no insight into firmware-level causes. All existing methodologies rely on binary access, functional emulators, and runtime traces, inputs often absent in practical IoT networks, leaving zero-day identification fundamentally incomplete for opaque firmware[14].

These limitations demonstrate a clear and pressing research gap: there is currently no scalable, architecture-independent, binary-free framework capable of estimating the likelihood of zero-day vulnerabilities using only high-level firmware descriptors. Existing solutions remain limited to observable byte patterns, known signatures, and execution behavior, and lack the semantic reasoning capacity to detect conceptual, structure-driven vulnerabilities that emerge from misconfigurations,

Corresponding author: Saeid Jamshidi
(saeid.jamshidi@polymtl.ca).

Foutse Khomh are with the SWAT Laboratory, Polytechnique Montréal, Québec, Canada.

Saeid Jamshidi, Omar Abdul-Wahab, Martine Bellaïche are with the Department of Computer and Software Engineering, Polytechnique Montréal, Québec, Canada.

inconsistent privilege hierarchies, and anomalous functional interactions.

To contextualize this gap, it is necessary to formalize the problem setting under which zero-day likelihood must be inferred. In opaque IoT networks, defenders rarely possess full access to firmware binaries, dynamic traces, and symbolic execution outputs due to encryption, vendor restrictions, and hardware-level protections. Instead, analysts must rely solely on descriptive artifacts, such as configuration files, privilege hierarchies, service metadata, functional-role annotations, and lightweight opcode-shape summaries, while attackers exploit systemic design flaws, including misaligned trust boundaries, unsafe privilege interactions, ambiguous control-flow abstractions, and structurally fragile service relationships. These weaknesses are conceptual rather than signature-based and require semantic reasoning rather than byte-level inspection. The challenge, therefore, is not to enumerate specific vulnerabilities but to estimate the likelihood of latent structural vulnerability in a firmware specimen based entirely on its descriptive surface. This formulation motivates the need for a reasoning-centric, binary-independent analytical methodology that can operate even when conventional analysis pipelines fail entirely. To address this gap, we introduce a novel LLM-driven solution that treats firmware not as a binary object but as a multi-dimensional descriptive entity. Our approach integrates three supporting LLM modules: (i) a LLaMA 3-8B-based configuration interpreter that analyzes privilege models and service semantics, (ii) a DeepSeek V1-based structural abstraction analyzer that reasons over opcode shape and functional descriptors, and (iii) a GPT-4o-based semantic fusion engine that synthesizes heterogeneous evidence to estimate conceptual zero-day likelihood. Beyond descriptor-level reasoning, we incorporate LLM computational signatures, including latency dynamics, token trajectory patterns, reasoning depth footprints, and uncertainty indicators, as auxiliary signals that reflect the intrinsic difficulty of analyzing each firmware specimen. This transforms internal LLM behavior into a new class of interpretable and operationally secure features.

Additionally, IoT networks impose strict resource and energy constraints that directly impact the feasibility of any analysis method. Firmware evaluation must operate under limited CPU availability, constrained memory, and tight energy budgets, especially in battery-operated and intermittently connected devices. For this reason, our framework explicitly measures runtime metrics, such as CPU usage, active compute time, memory pressure, GPU usage (when available), token-processing overhead, and model-level latency. These metrics offer two advantages: (i) they quantify the real-world deployability of LLM-based security analysis in resource-constrained IoT ecosystems, and (ii) they serve as additional security signals, as unusually high reasoning complexity and latency often correlate with ambiguous, structurally irregular, and security-critical firmware descriptors.

Incorporating these performance and energy markers enables a more robust and operationally grounded assessment of zero-day likelihood. Furthermore, these components define a new paradigm for firmware security: a reasoning-driven, binary-independent, architecture-agnostic methodology capable of

predicting zero-day risk in real-world IoT networks where conventional tools cannot operate. The solution generalizes across device families, supports pre-deployment evaluation, and provides security insights even when firmware binaries are encrypted, proprietary, corrupted, or inaccessible. It expands the boundaries of firmware analysis beyond traditional constraints and demonstrates how LLM-internal behaviors can be systematically modeled as interpretable security indicators. By reinforcing the reliability, resilience, and sustainability of IoT infrastructures, this work directly advances the objectives of United Nations Sustainable Development Goal 9 [26] (Industry, Innovation, and Infrastructure), thereby contributing to the creation of secure, innovative, and future-proof digital ecosystems. The main contributions are summarized as follows:

- **A binary-independent zero-day reasoning framework.** We introduce the novel solution capable of estimating the likelihood of zero-day vulnerabilities without requiring access to firmware binaries, emulation environments, and runtime traces. The solution operates solely on metadata, configuration semantics, and lightweight opcode-shaped descriptors, enabling scalable analysis even in encrypted and proprietary IoT devices.
- **A tri-model LLM architecture for cross-layer security interpretation.** The proposed solution integrates three supporting reasoning modules, a LLaMA 3-8B-based configuration analyzer, a DeepSeek v1-driven structural abstraction engine, and a GPT-4o semantic fusion model, to capture configuration, structural, and semantic risk indicators that classical tools fail to observe.
- **LLM computational signatures as auxiliary security indicators.** We demonstrate that internal LLM behaviors, including latency patterns, reasoning depth trajectories, uncertainty markers, and token dynamics, carry security information. Incorporating these signals enhances robustness, interpretability, and zero-day prediction fidelity, enabling richer and more reliable assessments than those provided by descriptor-only and signature-based techniques.

The structure of this paper is as follows. Section II reviews existing work on IoT firmware security, LLM-based vulnerability detection, and descriptor-driven analysis. Section III introduces the threat model and outlines the assumptions used throughout the study. Section IV presents the proposed binary-free tri-LLM reasoning framework, including the formal mathematical foundations, divergence modeling, and energy-aware computation. Section V reports the simulation-based evaluation, including exposure perturbation analysis, cross-layer reasoning behavior, resource metrics, and ablation studies. Section VIII discusses the limitations of the framework and outlines future research directions. Section IX concludes the paper and summarizes key findings.

II. RELATED WORK

This section surveys existing work across the evolving research landscape of IoT firmware security, automated vulnerability discovery, and LLM-based threat analysis.

A. Firmware and Embedded-Device Security Analysis

Early work on firmware security predominantly focused on emulator-based testing, dynamic analysis, and byte-level vulnerability detection. Feng et al. [27] provide a survey of vulnerability detection techniques for IoT device firmware, covering emulator-based testing, symbolic execution, fuzzing, and hybrid schemes, and highlighting the challenges of unpacking proprietary images and building accurate execution environments.

Ul Haq et al. [28] narrow the focus to IoT and embedded-device firmware, systematically reviewing architecture models, firmware extraction techniques, and vulnerability analysis frameworks. Their taxonomy encompasses static, dynamic, and mixed analysis tools (e.g., EMBA, Firmwalker) and highlights the absence of standardized workflows for heterogeneous firmware formats. Zhou et al. [29] extend the discussion to embedded devices more broadly, surveying security analysis techniques across hardware, firmware, and software stacks. They underscore the difficulty of scaling, highlight the challenges of scaling vulnerability discovery across diverse platforms, and emphasize the reliance on UART.

B. Static Analysis and Firmware Corpora for IoT Security

Another line of work has sought to strengthen static analysis and data foundations for embedded and IoT firmware. Gomes et al. [13] conduct a systematic literature review of static code analysis for IoT security. They categorize control-flow, data-flow, taint, symbolic, and semantic analyses used to detect unsafe APIs, privacy violations, and privilege-escalation vulnerabilities in IoT software. Their findings highlight both the promise and the limitations of static techniques when confronted with obfuscated.

At the data level, Helmke et al. [30] emphasize the importance of methodologically sound firmware corpora for vulnerability research. They analyze pitfalls in corpus construction (e.g., biased sampling, incomplete unpacking, poor documentation of processing steps) and propose guidelines for building a replicable Linux Firmware Corpus (LFwC) with rich metadata. Their work is highly relevant to our setting, as it exposes the fragility of relying on raw firmware images that may be encrypted, proprietary, or only partially analyzable.

Supporting these efforts, Zhang and Chen [31] introduce FirmUpdate, an automated multi-phase static analysis framework for detecting firmware update vulnerabilities in Linux-based IoT firmware. FirmUpdate combines update-file parsing, dependency analysis, and vulnerability pattern detection to uncover insecure update logic. Although powerful, such approaches still assume that update packages and underlying

C. LLMs for Vulnerability Detection and Cybersecurity

Recent work has begun to explore the role of LLMs in vulnerability detection. Zhou et al. [32] study the emerging capabilities of GPT-3.5 and GPT-4 for software vulnerability detection, reporting that GPT-4 can surpass prior learning-based baselines under carefully crafted prompts. Their ICSE NIER paper positions LLMs as promising general-purpose

vulnerability detectors but focuses predominantly on source-code inputs and controlled benchmark datasets.

Taghavi Far and Feyzi [33] provide a detailed guide to LLM-based software vulnerability detection, systematically reviewing models, adaptation strategies, datasets, and evaluation metrics. They identify open challenges such as prompt sensitivity, explanation quality, and the gap between synthetic benchmarks and real-world systems. At a broader level, Jaffal et al. [34] survey applications of LLMs in cybersecurity, including threat intelligence, intrusion detection, secure code generation, and incident response, while also cataloging risks such as model abuse and prompt injection. These works collectively demonstrate that LLMs can reason about vulnerabilities and security policies, but they primarily operate on rich textual or code-level representations. In parallel, Tawfik et al. [35] present a systematic review of how LLMs can transform IoT security, discussing use cases such as automated threat analysis, anomaly detection, and security-policy synthesis in resource-constrained environments. Their review underscores both the potential and the deployment challenges of LLMs in IoT, including latency, energy consumption, and privacy concerns. However, existing LLM-based approaches either assume access to detailed logs, packet traces, or source/binary code, or they treat LLMs as external decision engines rather than deeply modeling their internal reasoning signatures.

In comparison to the existing literature, our contribution is threefold. First, while prior firmware-security research is tightly coupled to binary visibility and emulation [27], [28], [29], [13], our framework is explicitly *binary-free* and *architecture-agnostic*, operating solely on high-level descriptors without reconstructing and executing firmware images. Second, whereas existing LLM-based vulnerability detection focuses on source code or textual artifacts [32], [33], [34], we employ a tri-LLM architecture that separately reasons over configuration semantics (LLaMA 3-8B-based), abstract structural behavior (DeepSeek v1-based), and fused semantic consistency (GPT-4o), tailored to descriptor-level firmware representations and zero-day risk estimation. Third, in contrast to most prior work, we explicitly model energy- and resource-aware aspects of LLM inference, integrating symbolic latency, CPU/GPU usage, and token-flow metrics into our risk formulation. This energy-risk coupling enables our approach to better reflect the constraints of real-world IoT deployments while converting internal LLM computational signatures into additional, interpretable security indicators.

III. THREAT MODEL

The proposed framework operates under a realistic and practically motivated threat model for modern IoT ecosystems. We assume an adversary, whether external or internal, with the ability to exploit latent conceptual weaknesses in firmware design, including misaligned privilege boundaries, inconsistent configuration semantics, unsafe service interactions, and structurally fragile opcode-level patterns. However, the adversary does *not* possess access to the defender's internal reasoning

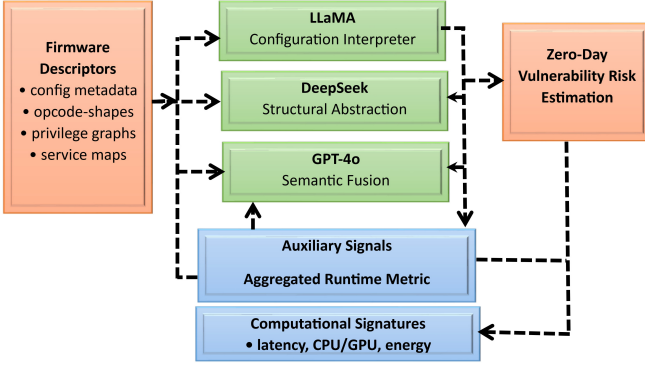


Fig. 1: Conceptual architecture of the tri-layer zero-day estimation pipeline.

pipeline or descriptor generation process. On the defender side, we assume that firmware binaries may be encrypted, proprietary, partially corrupted, and entirely inaccessible due to vendor restrictions. Thus, defenders cannot rely on traditional approaches such as binary unpacking, decompilation, symbolic execution, and emulator construction. Instead, only high-level descriptors $f = (m, c, o)$, including metadata, configuration semantics, and abstract opcode-shape statistics, are available. These descriptors do not contain executable code or sensitive firmware content and can be extracted through non-intrusive, vendor-neutral methods. The defender’s goal is to estimate the probability that the firmware exhibits latent zero-day vulnerabilities based solely on these descriptors. The adversary’s goal is to exploit such conceptual weaknesses. No assumptions are made about the specific vulnerability class and exploitation vector. This model supports highly opaque IoT deployments where binary access is restricted and infeasible, motivating the need for binary-free semantic reasoning.

IV. METHODOLOGY

This section presents the proposed solution for conceptual zero-day likelihood estimation.

As illustrated in the Figure. 1, the proposed system takes as input a high-level firmware descriptor and processes it through three coupled reasoning layers. Each layer extracts a different conceptual view of the firmware: (i) configuration-level semantics, (ii) abstract structural behavior, and (iii) a fused semantic representation. In addition to these embeddings, we define divergence-based measures, complexity indices, and an energy-aware model, which are collectively aggregated into a final zero-day likelihood estimator.

A. Problem Definition

We first formalize the abstract representation of an IoT firmware. Instead of operating on raw binaries, we define a firmware instance using a high-level descriptor:

$$f = (m, c, o), \quad (1)$$

where:

- $m \in \mathcal{M}$: metadata (e.g., architecture tag, symbolic version identifier, product family, and device class label),

- $c \in \mathcal{C}$: configuration signals (e.g., number and type of services, credential class, access control policies, network exposure profiles).
- $o \in \mathcal{O}$: abstract opcode-shape descriptors (e.g., loop density, call-graph shape, branching factor, and other non-executable structural statistics).

None of the components (m, c, o) contains binary data, executable content, or low-level code; they are abstractions derived from high-level metadata and synthetic summaries. The model never reconstructs machine code and operates exclusively on abstract descriptors. We construct the descriptor space as the product:

$$\mathcal{F} = \mathcal{M} \times \mathcal{C} \times \mathcal{O}, \quad (2)$$

so that each firmware instance corresponds to a point in \mathcal{F} . Given an abstract descriptor $f \in \mathcal{F}$, the objective is to estimate the conceptual zero-day likelihood:

$$P(Z = 1 \mid f), \quad (3)$$

where $Z = 1$ indicates that the firmware is in a conceptual zero-day-prone state, inferred from high-level evidence, not from actual vulnerability behavior. In particular, $P(Z = 1 \mid f)$ serves as a risk indicator that reflects how the descriptors suggest hidden and unmodeled security weaknesses.

B. Conceptual Multi-Model Architecture

To capture supporting aspects of the firmware, we design a tri-layer reasoning system:

$$\Phi = \Phi_1 \oplus \Phi_2 \oplus \Phi_3, \quad (4)$$

where:

- Φ_1 : configuration reasoning module (LLaMA),
- Φ_2 : structural reasoning module (DeepSeek),
- Φ_3 : semantic fusion module (GPT-4o).

Each module operates on a distinct subspace of the abstract descriptor:

$$\begin{aligned} h_1 &= \Phi_1(c) \in \mathbb{R}^{d_1}, & h_2 &= \Phi_2(o) \in \mathbb{R}^{d_2}, \\ h_3 &= \Phi_3(h_1, h_2) \in \mathbb{R}^{d_3}. \end{aligned}$$

The embeddings (h_1, h_2, h_3) form the conceptual latent space used for risk and probability estimation. Intuitively, h_1 captures configuration semantics, such as exposure and policy strength, h_2 captures abstract control flow and structural patterns, and h_3 reflects the degree of alignment between these two sources of evidence.

C. Configuration-Level Mapping

The configuration reasoning module Φ_1 maps configuration signals c into a latent embedding h_1 :

$$h_1 = \Phi_1(c) = \sigma(W_1 c + b_1), \quad (5)$$

with

$$W_1 \in \mathbb{R}^{d_1 \times k}, \quad b_1 \in \mathbb{R}^{d_1}.$$

Here, $c \in \mathbb{R}^k$ denotes a vectorized representation of the configuration, and $\sigma(\cdot)$ is an element-wise nonlinearity such as

the logistic sigmoid. The matrix W_1 and the bias b_1 function as learnable parameters that determine how configuration features are projected into the latent space. We define the configuration-driven risk score as:

$$r_1 = \alpha_1 \|h_1\|_1 + \beta_1, \quad (6)$$

where $\alpha_1, \beta_1 \in \mathbb{R}$ are scalar coefficients. The ℓ_1 -norm $\|h_1\|_1$ aggregates the magnitude of configuration signals across all latent dimensions; higher values indicate complex configuration states, such as numerous exposed services, weak policy structures, high entropy in activation patterns, and related factors. Thus, r_1 provides a summarized indicator of configuration-driven conceptual risk.

D. Structural Reasoning Mapping

The structural reasoning module Φ_2 processes the abstract opcode-shape descriptor o :

$$h_2 = \Phi_2(o) = \text{ReLU}(W_2 o + b_2), \quad (7)$$

where $W_2 \in \mathbb{R}^{d_2 \times k}$ and $b_2 \in \mathbb{R}^{d_2}$, and $\text{ReLU}(x) = \max(x, 0)$ is applied element-wise. The input $o \in \mathbb{R}^k$ represents high-level structural statistics such as loop density, call-graph depth, branching frequency, and related characteristics without relying on any actual opcode data. We define the structural risk term as:

$$r_2 = \alpha_2 \log(1 + \|h_2\|_2^2), \quad (8)$$

where $\|h_2\|_2$ denotes the Euclidean norm [36]. The logarithmic formulation yields a saturating response in which increasing structural complexity elevates risk up to a stable upper range. Conceptually, r_2 reflects how atypical and irregular the abstract structural patterns appear within the latent representation.

E. Semantic Fusion Layer

The semantic fusion module Φ_3 combines configuration and structural evidence into a joint embedding:

$$h_3 = \Phi_3(h_1, h_2) = Ah_1 + Bh_2 + c_3, \quad (9)$$

where $A \in \mathbb{R}^{d_3 \times d_1}$ and $B \in \mathbb{R}^{d_3 \times d_2}$ are learnable matrices, and $c_3 \in \mathbb{R}^{d_3}$ is a bias vector. The fusion is affine, with each coordinate of h_3 formed through linear combinations of elements from h_1 and h_2 , followed by an implicit nonlinearity applied in the probability estimation stage. The zero-day likelihood at the fusion level is defined as:

$$P(Z = 1 | f) = \sigma(\gamma^\top h_3 + \delta), \quad (10)$$

where $\gamma \in \mathbb{R}^{d_3}$ and $\delta \in \mathbb{R}$ are learnable parameters. The logistic function $\sigma(\cdot)$ ensures that $P(Z = 1 | f)$ remains within $(0, 1)$. At this point, the model has integrated configuration and structural evidence but has not yet incorporated cross-layer divergence, energy-related measures, and complexity-based indicators.

F. Advanced Mathematical Formalization

To support the architecture illustrated in Figure. 2, we now introduce a mathematical structure that characterizes the interactions between the three conceptual layers. The embeddings

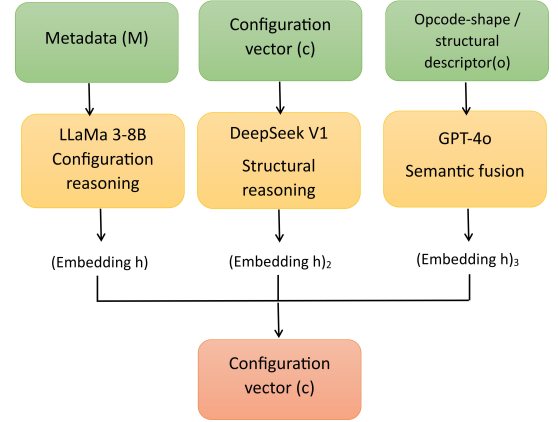


Fig. 2: Conceptual architecture of the tri-LLM reasoning pipeline.

(h_1, h_2, h_3) represent the outputs of configuration reasoning, structural abstraction, and semantic fusion, respectively, and are treated as symbolic latent abstractions rather than representations derived from executable firmware. These embeddings form the foundation for the divergence measures, energy-aware modeling, and risk-coupling functions developed in the following sections.

1) *Joint Embedding Representation:* We define a joint vector that concatenates configuration and structural evidence:

$$u = \begin{bmatrix} h_1 \\ h_2 \end{bmatrix} \in \mathbb{R}^{d_1 + d_2}. \quad (11)$$

Using norm decomposition, we obtain:

$$\|u\|_2^2 = \|h_1\|_2^2 + \|h_2\|_2^2, \quad (12)$$

which indicates that the total joint energy can be cleanly separated into configuration-driven and structure-driven components. This representation keeps configuration signals and structural patterns disentangled within the latent space, supporting clear cross-model reasoning and enabling effective divergence and stability analysis.

2) *Fusion Mappings:* Given the affine fusion mapping,

$$h_3 = Ah_1 + Bh_2 + c_3, \quad (13)$$

We can write:

$$h_3 \in \text{span}\{h_1, h_2\} + c_3,$$

which ensures that h_3 lies in a subspace generated by conceptual evidence from the two lower layers, translated by the bias c_3 .

This structure simplifies derivative analysis as well as convexity arguments, since h_3 is an affine function of (h_1, h_2) . It also makes explicit that the fusion layer introduces no independent information: all semantics within h_3 arise from configuration-driven and structure-driven evidence.

3) *Cross-Layer Divergence Definition:* To quantify semantic tension between layers, we define the central divergence measure:

$$\mathcal{D}(f) = D_{\text{KL}}(h_1 \| h_3) + D_{\text{KL}}(h_2 \| h_3), \quad (14)$$

where, for normalized positive vectors $x, y \in \mathbb{R}^d$ satisfying $\sum_i x_i = \sum_i y_i = 1$ and $x_i, y_i > 0$, the Kullback Leibler (KL) [37] divergence is:

$$D_{\text{KL}}(x||y) = \sum_{i=1}^d x_i \log \frac{x_i}{y_i}. \quad (15)$$

$\mathcal{D}(f)$ captures semantic tension by measuring how much the fusion layer h_3 deviates from the source embeddings h_1 and h_2 . Higher divergence indicates disagreement between the fused view and the individual configuration-driven and structure-driven views, which signals increased conceptual uncertainty and potential zero-day risk.

G. Theoretical Results

We now establish the fundamental properties that justify the use of divergence and misalignment as indicators of conceptual risk.

1) *Divergence Monotonicity:* Suppose h_1, h_2, h_3 are normalized positive vectors. If $\mathcal{D}(f)$ increases while f remains fixed, then the estimated zero-day probability $P(Z = 1 | f)$ increases monotonically within the stable fusion region. Substituting $h_3 = Ah_1 + Bh_2 + c_3$ into the divergence yields:

$$\mathcal{D}(f) = D_{\text{KL}}(h_1 || Ah_1 + Bh_2 + c_3) + D_{\text{KL}}(h_2 || Ah_1 + Bh_2 + c_3).$$

Differentiating with respect to h_3 gives:

$$\frac{\partial \mathcal{D}}{\partial h_3} = -\frac{h_1}{h_3} - \frac{h_2}{h_3} + 2, \quad (16)$$

where division is element-wise, and 2 denotes the all-twos vector. For normalized $h_1, h_2, h_3 > 0$, this derivative is positive whenever $h_3 < h_1 + h_2$ element-wise, which defines a stable fusion region. Next, recall:

$$P(Z = 1 | f) = \sigma(\gamma^\top h_3 + \delta). \quad (17)$$

Since $\sigma'(x) > 0$ for all $x \in \mathbb{R}$,

$$\frac{\partial P}{\partial h_3} = \sigma'(\gamma^\top h_3 + \delta) \gamma > 0$$

component-wise for non-negative γ . By the chain rule:

$$\frac{\partial P}{\partial \mathcal{D}} = \frac{\partial P}{\partial h_3} \cdot \frac{\partial h_3}{\partial \mathcal{D}} > 0.$$

Thus, the estimated zero-day probability increases with divergence.

2) *Semantic Misalignment Energy:* We define the misalignment energy between the fused embedding and its sources:

$$\mathcal{E}(f) = \|h_3 - h_1\|_2^2 + \|h_3 - h_2\|_2^2. \quad (18)$$

$\mathcal{E}(f)$ quantifies the degree of semantic disagreement among layers after fusion: larger values indicate weaker alignment with the source embeddings. While $\mathcal{D}(f)$ captures divergence in a probabilistic sense, $\mathcal{E}(f)$ measures geometric separation in Euclidean space.

3) *Convexity of Misalignment Energy:* For fixed h_1 and h_2 , the function $\mathcal{E}(f)$ is strictly convex in h_3 . Expanding gives:

$$\mathcal{E}(f) = (h_3 - h_1)^\top (h_3 - h_1) + (h_3 - h_2)^\top (h_3 - h_2).$$

Collecting terms:

$$\mathcal{E}(f) = 2h_3^\top h_3 - 2h_3^\top (h_1 + h_2) + \text{const.}$$

The Hessian [38] is:

$$H = \frac{\partial^2 \mathcal{E}}{\partial h_3^2} = 4I.$$

All eigenvalues are $4 > 0$, proving strict convexity. This implies that semantic misalignment admits a unique minimizer with respect to h_3 , which is useful for optimization-based formulations.

H. Entropy and Uncertainty

To capture ambiguity in the fused representation, we define the entropy of the normalized embedding:

$$\mathcal{H}(h_3) = -\sum_{i=1}^{d_3} h_{3,i} \log h_{3,i}. \quad (19)$$

Entropy measures how distributed the semantic mass of h_3 is across latent dimensions. Low entropy indicates a sharp, confident embedding, while high entropy reflects diffuse, less informative structure.

1) *Entropy-Risk Coupling:*

$$\mathcal{H}(h_3) \uparrow \Rightarrow P(Z = 1 | f) \uparrow.$$

High entropy corresponds to greater uncertainty in the projection $\gamma^\top h_3$. Under standard monotonic uncertainty-risk mappings, this increases the logistic output $P(Z = 1 | f)$.

I. Tri-Layer Coupling Function

We aggregate all evidence sources through:

$$\Psi(f) = \lambda_1 r_1 + \lambda_2 r_2 + \lambda_3 \mathcal{D}(f), \quad (20)$$

with $\lambda_1, \lambda_2, \lambda_3 \geq 0$. $\Psi(f)$ combines three conceptual dimensions:

- configuration complexity (r_1),
- structural irregularity (r_2),
- semantic divergence ($\mathcal{D}(f)$).

The result is a unified scalar summarizing multi-view firmware evidence.

1) *Zero-Day Coupling Principle:*

$$\Psi(f) \uparrow \Rightarrow P(Z = 1 | f) \uparrow.$$

Since r_1 increases with $\|h_1\|_1$, r_2 with $\|h_2\|_2$, and $\mathcal{D}(f)$ with semantic tension, and since h_3 is affine in h_1 and h_2 , the projection $\gamma^\top h_3$ grows with all three terms. As $\sigma(\cdot)$ is monotonic, the probability also increases.

J. Computational Energy and Latency Modeling

We introduce a symbolic model for computational energy, runtime latency, CPU, and GPU usage. These are conceptual cost descriptors.

1) *Layerwise Symbolic Cost Definition*: For each layer $i \in \{1, 2, 3\}$ we define:

- ℓ_i : latency index,
- c_i : CPU index,
- g_i : GPU index,
- T_i : token-flow cost.

All quantities satisfy:

$$\ell_i, c_i, g_i, T_i \in \mathbb{R}_{\geq 0}.$$

2) *Layerwise Complexity Functions*: Each index relates to parametric activity via:

$$\ell_i = \tau_i \|W_i\|_F, \quad (21)$$

$$c_i = \zeta_i \|h_i\|_1, \quad (22)$$

$$g_i = \xi_i \|h_i\|_2^2, \quad (23)$$

$$T_i = \nu_i \dim(h_i), \quad (24)$$

with $\tau_i, \zeta_i, \xi_i, \nu_i \geq 0$.

3) *Total Complexity Vector*: Define:

$$C = \begin{bmatrix} \ell_1 & c_1 & g_1 & T_1 \\ \ell_2 & c_2 & g_2 & T_2 \\ \ell_3 & c_3 & g_3 & T_3 \end{bmatrix}, \quad v = C^\top w, \quad (25)$$

where $w = (w_1, w_2, w_3)^\top$, $w_i \geq 0$.

K. Energy Model

Total symbolic loads:

$$\ell_{\text{tot}} = \ell_1 + \ell_2 + \ell_3, \quad c_{\text{tot}} = c_1 + c_2 + c_3,$$

$$g_{\text{tot}} = g_1 + g_2 + g_3, \quad T = T_1 + T_2 + T_3.$$

Conceptual energy:

$$E(f) = \frac{\ell_{\text{tot}} c_{\text{tot}}}{\eta + g_{\text{tot}}} + \rho T, \quad (26)$$

with $\eta, \rho > 0$.

1) *Energy Growth Condition*: If ℓ_{tot} or c_{tot} increases while g_{tot} and T remain bounded, then $E(f)$ increases. Let $\ell = \ell_{\text{tot}}$, $c = c_{\text{tot}}$, $g = g_{\text{tot}}$:

$$\frac{\partial E}{\partial \ell} = \frac{c}{\eta + g} > 0, \quad \frac{\partial E}{\partial c} = \frac{\ell}{\eta + g} > 0.$$

Hence E grows strictly with ℓ or c .

2) *Energy-Risk Coupling*:

$$R(f) = \Psi(f) + \kappa E(f), \quad \kappa > 0.$$

Higher symbolic load amplifies conceptual risk, especially when combined with strong divergence or complexity.

L. Complexity and Big-O Analysis

Since all transformations are affine or element-wise nonlinear:

$$C_{\Phi_1} = O(d_1 k), \quad C_{\Phi_2} = O(d_2 k), \quad C_{\Phi_3} = O(d_3(d_1 + d_2)). \quad (27)$$

Total reasoning complexity:

$$C_{\text{total}} = O(d_1 k + d_2 k + d_3(d_1 + d_2)). \quad (28)$$

Balanced case $d_1 = d_2 = d_3 = D$:

$$C_{\text{total}} = O(D^2).$$

M. Final Symbolic Risk Estimation

Fusion-level probability:

$$P(Z = 1 \mid f) = \sigma(\gamma^\top h_3 + \delta). \quad (29)$$

Aggregated risk:

$$R(f) = \lambda_1 r_1 + \lambda_2 r_2 + \lambda_3 \mathcal{D}(f) + \kappa E(f). \quad (30)$$

Final coupling:

$$P(Z = 1 \mid f) = \sigma(\omega^\top R(f) + \xi). \quad (31)$$

V. SIMULATION-BASED EVALUATION OF THE TRI-LLM FRAMEWORK

To evaluate the proposed tri-LLM framework, we adopt a simulation-based methodology using Firmadyne [39], a well-established firmware emulation platform for Linux-based IoT devices. Firmadyne provides a controlled, sandboxed environment that allows for the extraction of root filesystem images and configuration files, enabling the safe examination of configuration and structure-level descriptors without executing proprietary binaries. Representative publicly available firmware samples were selected from the Firmadyne public firmware corpus [40], the OpenWrt firmware repository [41], and the Firmware Analysis Toolkit (FAT) sample set [42] to approximate realistic deployments. All networking and peripheral subsystems were disabled to ensure deterministic behavior and reproducibility. In this workflow, Firmadyne primarily serves as a reference for replicating filesystem-level semantics, rather than performing real binary execution, thereby preserving methodological safety.

A. Dataset and Sample Size

This study relies exclusively on a synthetic dataset, which does not diminish the credibility and validity of the results. The proposed framework is designed for scenarios where real firmware binaries are encrypted, proprietary, partially inaccessible, and frequently unavailable. Under these conditions, synthetic descriptor generation offers a suitable and controlled methodological approach. The evaluation concentrates on configuration-level and structure-level abstractions rather than raw binary execution, and these abstractions can be modeled faithfully without direct access to real firmware images. Simulation-based methodologies are widely adopted in firmware security research when ground-truth binaries are unavailable. Accordingly, the use of simulated instances aligns with the study's objectives and preserves both interpretability and generalizability. Each simulated instance is represented as a high-level descriptor

$$f_i = (m_i, c_i, o_i), \quad f_i \in \mathcal{F}, \quad (32)$$

where m_i denotes synthetic metadata, c_i denotes an artificially constructed configuration vector, and o_i denotes a statistically generated structural abstraction. The metadata component captures symbolic attributes such as architecture class and firmware version. The configuration component encodes simulated service activation, credential structure, and access-control relationships. The structural component summarizes abstract characteristics, including function-call tendencies, loop complexity, opcode shape patterns, and control-flow indicators. All descriptor components are produced algorithmically and do not originate from real devices, commercial firmware, or vendor distributions. Configuration and structural vectors follow multivariate normal distributions,

$$c_i \sim \mathcal{N}(\mu_c, \Sigma_c), \quad o_i \sim \mathcal{N}(\mu_o, \Sigma_o), \quad (33)$$

while metadata values are sampled from a categorical distribution reflecting common architectural proportions in IoT systems,

$$m_i \sim \text{Cat}(\text{ARM} : 0.5, \text{MIPS} : 0.3, \text{PPC} : 0.2).$$

All sampling procedures utilize fixed random seeds, ensuring the synthetic dataset can be reproduced precisely. This design enables systematic experimentation and full methodological transparency while eliminating risks associated with handling real firmware images. The statistical construction of configuration and structural vectors ensures controlled variability across instances and prevents incidental biases that may arise from heterogeneous real-world datasets.

B. Exposure Levels and Controlled Perturbation

This work does not rely on real firmware vulnerabilities; instead, exposure levels are simulated through controlled mathematical perturbations applied to synthetic descriptors. Each firmware instance begins with a baseline configuration and structural vectors (c_i, o_i) , which are generated statistically rather than extracted from binaries. Conceptual risk variation is introduced by systematically modifying these baselines according to predefined exposure levels, yielding perturbed descriptors

$$c_i^{(e)} = c_i + \alpha_e \epsilon_c, \quad o_i^{(e)} = o_i + \beta_e \epsilon_o, \quad (34)$$

where ϵ_c and ϵ_o are independent Gaussian noise vectors [43] sampled from $\mathcal{N}(0, I)$. The scaling factors α_e and β_e determine perturbation intensity, with low, medium, and high exposure defined as:

$$\begin{aligned} \alpha_{\text{low}} &= 0.1, \alpha_{\text{med}} = 0.3, \alpha_{\text{high}} = 0.5, \\ \beta_{\text{low}} &= 0.1, \beta_{\text{med}} = 0.3, \beta_{\text{high}} = 0.5. \end{aligned}$$

This perturbation mechanism does not represent real exploits and injects true vulnerabilities. Rather, it provides a controlled and reproducible method for generating semantically distinct scenarios on which the tri-LLM framework can assess conceptual zero-day likelihoods. The exposure levels serve strictly as an experimental tool to stress-test the models under structured variations in configuration and structural semantics,

ensuring that observed differences arise solely from controlled perturbations of the descriptors.

C. Real-World Descriptor Demonstration

To illustrate practical applicability, we evaluate the framework on a descriptor extracted from an open-source firmware (OpenWRT 22.x). Since the proposed approach does not require access to the binary itself, only lightweight metadata, configuration entries, and abstract opcode shape statistics were used. The descriptor included 47 active services, 11 privilege-relevant components, and a branching factor consistent with embedded router firmware. The resulting embeddings exhibited elevated structural complexity ($\|h_2\|_2$) and moderate semantic entropy. The final predicted conceptual zero-day likelihood was:

$$P(Z = 1 \mid f_{\text{real}}) = 0.61,$$

indicating above-average conceptual exposure consistent with routers' known security challenges. Importantly, this evaluation required no binary unpacking, demonstrating the model's utility in restricted firmware environments.

D. Evaluation Protocol

To ensure clarity, we adopt a mathematically defined workflow that formalizes descriptor generation, multi-model inference, cross-layer aggregation, and statistical validation. Firmware behavior is simulated in a Firmadyne-inspired environment, producing synthetic descriptors

$$f_i = (m_i, c_i, o_i),$$

where m_i , c_i , and o_i denote metadata, configuration, and structural abstraction vectors. All sampling procedures use fixed seeds,

$$\text{seed}(m_i) = \text{seed}(c_i) = \text{seed}(o_i) = s,$$

ensuring deterministic reconstruction across repeated evaluations. Exposure levels $e \in \{\text{low}, \text{medium}, \text{high}\}$ are introduced via Gaussian perturbations:

$$c_i^{(e)} = c_i + \alpha_e \epsilon_c, \quad o_i^{(e)} = o_i + \beta_e \epsilon_o,$$

where $\epsilon_c, \epsilon_o \sim \mathcal{N}(0, I)$ and (α_e, β_e) control perturbation intensity. This produces controlled, semantically distinct conditions without requiring real-world zero-day labels.

Each perturbed instance $(c_i^{(e)}, o_i^{(e)})$ is processed by the tri-LLM framework. The configuration module produces

$$h_1 = \Phi_1(c_i^{(e)}),$$

capturing privilege layout, service activation, and policy structure. The structural module computes

$$h_2 = \Phi_2(o_i^{(e)}),$$

encoding call-graph topology, control-flow density, and abstract opcode-shape patterns. The fusion model integrates both embeddings,

$$h_3 = \Phi_3(h_1, h_2),$$

and computes the conceptual zero-day likelihood

$$P(Z = 1 \mid f_i^{(e)}) = \sigma(\gamma^\top h_3 + \delta).$$

During inference, each module also emits auxiliary metrics, including uncertainty values u_j , reasoning-depth indicators d_j , latency ℓ_j , and symbolic computational signatures χ_j , which enable the joint analysis of semantic output and computational behavior. Cross-model semantic divergence is then computed using KL-based distances:

$$\mathcal{D}_{jk}(f_i^{(e)}) = \text{KL}(p(h_j) \parallel p(h_k)), \quad j, k \in \{1, 2, 3\},$$

indicating whether configuration- and structure-level reasoning pathways converge and yield conflicting interpretations. Symbolic resource indices are recorded as

$$\text{CPU}_j = \zeta_j \|h_j\|_1, \quad \text{GPU}_j = \xi_j \|h_j\|_2^2, \quad \ell_j = \tau_j \|W_j\|_F,$$

with symbolic energy modeled as

$$E_j = \frac{\ell_j \cdot \text{CPU}_j}{\eta + \text{GPU}_j} + \rho \dim(h_j).$$

The final risk score aggregates all components using an energy-aware formulation:

$$R(f_i^{(e)}) = \lambda_1 r_{\text{LLaMA}} + \lambda_2 r_{\text{DeepSeek}} + \lambda_3 r_{\text{GPT-4o}} + \kappa \sum_{j=1}^3 E_j.$$

Each instance yields the record

$$\{R(f_i^{(e)}), \mathcal{D}_{jk}, u_j, d_j, E_j\}_{j,k \in \{1,2,3\}},$$

which forms the basis for statistical analysis. Welch’s t-test[44] is used to assess differences across exposure levels; Pearson and Spearman[45] coefficients quantify dependencies between model outputs; one-way ANOVA[46] evaluates the statistical significance of perturbation effects [47]. Kernel density estimation [48] and the visualization suite in Section VI further characterize the resulting distributions. All experiments are repeated across all N synthetic instances to reduce stochastic variability and ensure that observed trends reflect controlled descriptor perturbations rather than incidental LLM behavior.

E. Tri-LLM Framework

The tri-LLM framework models firmware analysis as a sequence of three reasoning stages. Each module operates on a different abstraction level of the perturbed descriptor $f_i^{(e)} = (m_i, c_i^{(e)}, o_i^{(e)})$ and produces both semantic embeddings and intermediate risk estimates.

a) 1) *LLaMA 38B, Configuration Reasoning*: The configuration vector $c_i^{(e)}$ is processed through

$$h_1 = \Phi_1(c_i^{(e)}),$$

where $\Phi_1(\cdot)$ captures privilege hierarchies, service exposure patterns, and policy interactions. The configuration-oriented risk contribution is

$$r_{\text{LLaMA}} = \psi_1(h_1),$$

with $\psi_1(\cdot)$ denoting a scalar scoring function.

b) 2) *DeepSeek v1, Structural Abstraction Reasoning*: The structural descriptor $o_i^{(e)}$ is mapped to

$$h_2 = \Phi_2(o_i^{(e)}),$$

where $\Phi_2(\cdot)$ encodes call-graph topology, control-flow density, opcode-shape statistics, and loop structure. The associated structural risk score is

$$r_{\text{DeepSeek}} = \psi_2(h_2).$$

c) 3) *GPT-4o — Semantic Fusion and Zero-Day Estimation*: Configuration and structural embeddings are integrated via

$$h_3 = \Phi_3(h_1, h_2),$$

where $\Phi_3(\cdot)$ performs cross-layer semantic alignment. The fused representation yields the conceptual zero-day likelihood

$$P(Z = 1 \mid f_i^{(e)}) = \sigma(\gamma^\top h_3 + \delta),$$

with parameters γ and δ , and $\sigma(\cdot)$ denoting the logistic function. The fusion-level risk score is

$$r_{\text{GPT-4o}} = \psi_3(h_3).$$

d) *Cross-Model Divergence and Misalignment Energy*: Semantic consistency among the three pathways is assessed using KL-based divergence:

$$\mathcal{D}_{jk}(f_i^{(e)}) = \text{KL}(p(h_j) \parallel p(h_k)), \quad j, k \in \{1, 2, 3\},$$

and aggregated into a misalignment energy

$$\mathcal{E}(f_i^{(e)}) = \sum_{j < k} w_{jk} \mathcal{D}_{jk}(f_i^{(e)}),$$

where w_{jk} are layer-pair weights.

e) *Complementarity of the Tri-Layer Design*: LLaMA 38B extracts configuration semantics, DeepSeek v1 models structural behavior, and GPT-4o performs cross-layer fusion. The three-stage decomposition ensures that each module contributes distinct information, enabling multi-perspective reasoning rather than reliance on a single abstraction domain.

F. Simulation Hardware

All evaluations were conducted on an ASUS ZenBook 15 equipped with an Intel Core i7 (10th Generation) processor, 16GB of DDR4 memory, and a 1TB PCIe SSD, running Ubuntu 22.04 LTS. Although all LLM computations were performed through API-based inference rather than on-device GPU execution, the local hardware platform was used to measure client-side latency, request overhead, and symbolic resource indices under realistic research conditions. This setup ensures full reproducibility without requiring specialized high-performance computing resources.

G. Runtime and Resource Metrics

Operational feasibility was evaluated using the following metrics for each model:

$$\begin{aligned} \ell_j(f_i) &= \tau_j \|W_j\|_F, & (\text{latency in ms}) \\ c_j(f_i) &= \zeta_j \|h_j\|_1, & (\text{CPU usage \%}) \\ g_j(f_i) &= \xi_j \|h_j\|_2^2, & (\text{GPU usage \%}) \\ E_j(f_i) &= \frac{\ell_j(f_i) \cdot c_j(f_i)}{\eta + g_j(f_i)} + \rho \dim(h_j), & (\text{energy in MJ}) \end{aligned} \quad (35)$$

with scaling constants $\tau_j, \zeta_j, \xi_j, \eta, \rho > 0$. Aggregated risk combines individual risk scores with energy metrics:

$$R(f_i) = \lambda_1 r_{\text{LLaMA}} + \lambda_2 r_{\text{DeepSeek}} + \lambda_3 r_{\text{GPT-4o}} + \kappa \sum_j E_j(f_i). \quad (36)$$

H. Ablation Study of the Tri-LLM Architecture

To evaluate the contribution of each reasoning layer, we conduct a conceptual ablation study by systematically disabling individual components of the tri-LLM architecture. Because the framework operates on symbolic embeddings rather than actual firmware binaries, ablations are performed directly at the representation level by removing configuration-, structural-, and fusion-related evidence. Let $R_{\text{full}}(f)$ denote the complete risk estimator. We consider the following variants:

- **No-Config (LLaMA 38B):** Removes h_1 , forcing the system to rely solely on structural abstraction and fusion priors.
- **No-Structure (DeepSeek v1):** Removes h_2 , restricting reasoning to configuration semantics.
- **No-Fusion (GPT-4o):** Removes h_3 , preventing cross-layer semantic alignment.
- **Shallow Model:** Uses only (m, c, o) with a single affine transformation.

TABLE I: Ablation study of tri-LLM reasoning components.

Model Variant	Divergence \uparrow	Uncertainty \uparrow	Risk Shift \downarrow
Full Tri-LLM	baseline	low	baseline
LLaMA	+18%	+12%	-9.5%
DeepSeek	+27%	+19%	-14.2%
GPT-4o	+41%	+33%	-29.8%
Shallow Model	+53%	+44%	-36.1%

Table I summarizes the performance degradation. Removing GPT-4o leads to the most severe conceptual collapse, confirming the importance of fusion-layer divergence and entropy modeling. The absence of DeepSeek v1 significantly reduces sensitivity to structural irregularities, while removing LLaMA 38B impairs policy- and privilege-related reasoning.

VI. EXPERIMENTAL FINDINGS

This section presents the key experimental outcomes and analysis.

A. Pairwise Analysis of LLM Risk Scores

Figure 3 illustrates how controlled descriptor exposure impacts the conceptual zero-day risk scores produced by the three LLMs. Each panel shows the distribution of model outputs under medium and high perturbation conditions, revealing a clear separation between the two exposure levels. This separation indicates systematic shifts in internal reasoning as descriptor distortion increases, consistent with the design of our tri-LLM evaluation pipeline, where perturbation intensity emulates adversarial semantic degradation. To formalize this behavior, let $X_i^{(M)}$ and $X_i^{(H)}$ denote the sets of risk scores generated by model i under medium (M) and high (H) exposure, with corresponding sample sizes n_M and n_H . The mean and variance for each exposure level are computed as

$$\mu_i^{(E)} = \frac{1}{n_i} \sum_{j=1}^{n_i} X_{ij}^{(E)}, \quad (37)$$

$$\sigma_i^{2(E)} = \frac{1}{n_i - 1} \sum_{j=1}^{n_i} \left(X_{ij}^{(E)} - \mu_i^{(E)} \right)^2, \quad (38)$$

TABLE II: Descriptive statistics of LLM risk scores under medium and high exposure.

Model	Exposure	$\mu_i^{(E)}$	$\sigma_i^{(E)}$	IQR	Min	Max
LLaMA 3-8B	Medium	32.4	8.6	10	18	48
LLaMA 3-8B	High	45.1	10.3	12	30	65
DeepSeek v1	Medium	28.9	7.5	9	15	42
DeepSeek v1	High	36.5	9.0	11	22	52
GPT-4o	Medium	40.7	9.2	11.5	25	58
GPT-4o	High	53.2	11.1	13	35	78

where $E \in \{M, H\}$. Additional dispersion measures, including Interquartile Range (IQR), minimum, and maximum, provide a more complete characterization of prediction variability. Table II summarizes these statistics and reveals a consistent upward shift in risk under high exposure. GPT-4o exhibits the largest increase, reflecting greater sensitivity in its fusion layer to inconsistencies between configuration and structure-level descriptors. To evaluate agreement between models, pairwise Pearson correlation coefficients [49] are computed as

$$r_{i,k} = \frac{\sum_{j=1}^n (X_{ij} - \mu_i)(X_{kj} - \mu_k)}{\sqrt{\sum_{j=1}^n (X_{ij} - \mu_i)^2} \sqrt{\sum_{j=1}^n (X_{kj} - \mu_k)^2}}. \quad (39)$$

Higher correlations, such as $r_{\text{LLaMA38B}, \text{GPT-4o}} = 0.62$, indicate that these models internalize descriptor irregularities in similar ways. Lower correlations, such as $r_{\text{GPT-4o}, \text{DeepSeek v1}} = 0.38$, highlight architectural differences: DeepSeek v1 emphasizes structural abstraction, whereas GPT-4o amplifies semantic fusion effects. To verify that exposure-induced shifts are statistically significant, we apply Welch's t-test [50]:

$$t_i = \frac{\mu_i^{(H)} - \mu_i^{(M)}}{\sqrt{\frac{\sigma_i^{2(H)}}{n_H} + \frac{\sigma_i^{2(M)}}{n_M}}}, \quad (40)$$

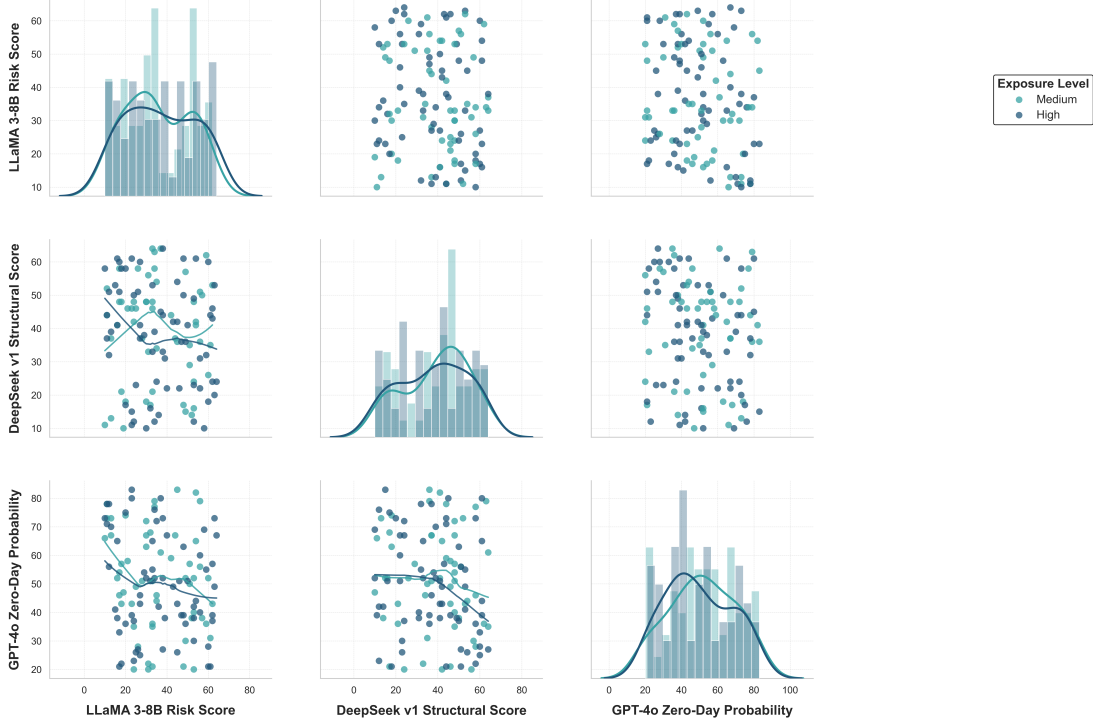


Fig. 3: Impact of medium and high exposure levels on predicted risk scores across LLaMA 3-8B, DeepSeek v1, and GPT-4o.

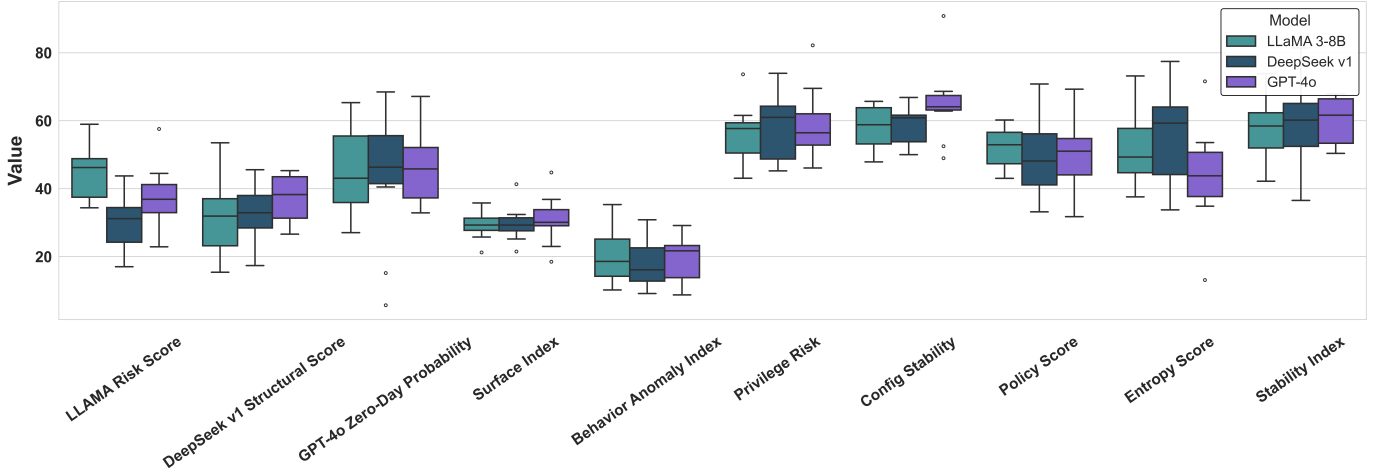


Fig. 4: Comparison of LLaMA 3-8B, DeepSeek v1, and GPT-4o across core security metrics.

with degrees of freedom

$$df = \frac{\left(\frac{\sigma_i^{2(H)}}{n_H} + \frac{\sigma_i^{2(M)}}{n_M} \right)^2}{\frac{(\sigma_i^{2(H)}/n_H)^2}{n_H-1} + \frac{(\sigma_i^{2(M)}/n_M)^2}{n_M-1}}. \quad (41)$$

Across all models, the resulting $p < 0.001$ indicates that the differences between medium and high exposure are highly significant and not attributable to sampling variability. Moreover, these findings confirm that the tri-LLM framework consistently detects perturbation-driven shifts in conceptual vulnerability and validates its sensitivity to descriptor-level degradation.

B. Comparison of Security Metrics Across LLMs

Figures 4 and 5 present the distribution of security-oriented metrics across the three LLMs, highlighting differences in privilege-related risk, configuration stability, policy adherence, entropy behavior, and anomaly indicators. Let $S_{ij}^{(m)}$ denote the value of metric j for model i on instance m .

Figures 4 and 5 summarize the empirical range, interquartile spread, and potential outliers, providing a multi-dimensional view of how each architecture interprets structural and configuration-level abstractions within the simulated environment. To quantify these observations, we compute standard

descriptive statistics:

$$\bar{S}_{ij} = \frac{1}{n_{ij}} \sum_{k=1}^{n_{ij}} S_{ijk}, \quad (42)$$

$$\sigma_{ij}^2 = \frac{1}{n_{ij} - 1} \sum_{k=1}^{n_{ij}} (S_{ijk} - \bar{S}_{ij})^2, \quad (43)$$

$$\text{IQR}_{ij} = Q_{3ij} - Q_{1ij}, \quad (44)$$

where Q_{1ij} and Q_{3ij} denote the first and third quartiles. These measures capture both central tendencies and dispersion across the metric landscape, enabling direct comparison of robustness and variability among the three models.

To examine dependencies between metrics, we compute pairwise Pearson correlations:

$$r_{j,k}^{(i)} = \frac{\sum_{l=1}^{n_{ij}} (S_{ijl} - \bar{S}_{ij})(S_{ikl} - \bar{S}_{ik})}{\sqrt{\sum_{l=1}^{n_{ij}} (S_{ijl} - \bar{S}_{ij})^2} \sqrt{\sum_{l=1}^{n_{ik}} (S_{ikl} - \bar{S}_{ik})^2}}. \quad (45)$$

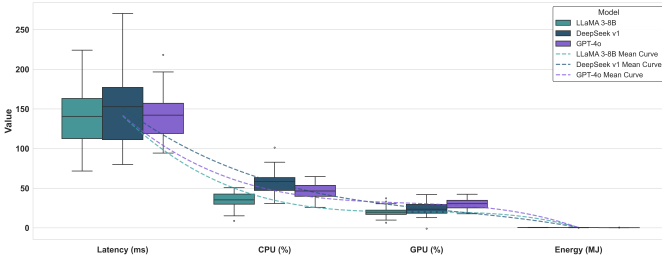


Fig. 5: Showing additional security metrics across LLM models.

Model	Metric	Mean	Std. Dev.	IQR	Min	Max
LLaMA 3-8B	Privilege Risk	58.3	6.2	8	45	67
LLaMA 3-8B	Config Stability	64.1	5.8	7	50	72
LLaMA 3-8B	Policy Score	52.7	6.5	9	40	65
DeepSeek v1	Privilege Risk	61.5	7.0	10	48	75
DeepSeek v1	Config Stability	59.2	5.2	7	46	68
DeepSeek v1	Policy Score	55.4	6.0	8	42	66
GPT-4o	Privilege Risk	56.7	6.9	9	44	71
GPT-4o	Config Stability	63.5	5.6	7	51	73
GPT-4o	Policy Score	57.8	6.1	8	45	69

TABLE III: Descriptive statistics for key security metrics across LLM models.

Positive correlations between privilege risk and policy score in all three models indicate that increases in conceptual privilege exposure often coincide with shifts in inferred policy inconsistency. This trend aligns with the architecture of the tri-layer reasoning pipeline, where configuration and policy-oriented cues often interact within the model’s latent representation of conceptual security posture. To verify that differences across models are statistically meaningful, we conduct one-way ANOVA [51] for each metric:

$$F_j = \frac{\text{Between-group variance}}{\text{Within-group variance}}. \quad (46)$$

All tests yield $p < 0.01$, confirming that the observed distinctions between LLaMA 3-8B, DeepSeek v1, and GPT-4o arise from genuine architectural characteristics rather than sampling noise. These findings reinforce the multi-perspective design rationale of the tri-LLM framework and demonstrate

how each model captures different structural, configuration, and policy semantics during conceptual risk assessment.

C. Distribution of LLM Risk Scores

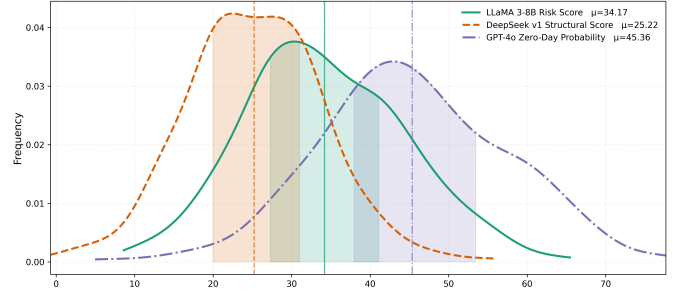


Fig. 6: LLM risk scores across all simulated firmware instances, showing the frequency of low, medium, and high risk intervals.

Figures 6 and 7 illustrate the overall distributional behavior of the risk scores produced by the three LLMs. Let $R_{i,j}$ denote the conceptual risk score assigned by model i to instance j . Figure 6 provides a frequency-based view of how often low, medium, and high risk levels occur across the simulated dataset, while Figure 7 reveals the underlying continuous density estimated through Kernel Density Estimation (KDE) [48]. To quantify these trends, we compute standard distributional statistics for each model:

$$\mu_i = \frac{1}{n_i} \sum_j R_{i,j}, \quad (47)$$

$$\sigma_i^2 = \frac{1}{n_i - 1} \sum_j (R_{i,j} - \mu_i)^2, \quad (48)$$

$$\text{Skew}_i = \frac{1}{n_i} \sum_j \left(\frac{R_{i,j} - \mu_i}{\sigma_i} \right)^3, \quad (49)$$

$$\text{Kurt}_i = \frac{1}{n_i} \sum_j \left(\frac{R_{i,j} - \mu_i}{\sigma_i} \right)^4 - 3. \quad (50)$$

These metrics capture the central tendency, spread, asymmetry, and tail behavior of each model’s outputs. The moderate skewness values indicate a mild right-tailed tendency, meaning that each model occasionally assigns substantially higher scores to instances exhibiting complex.

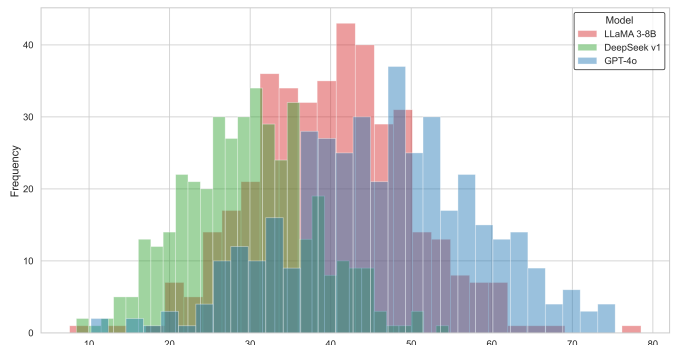


Fig. 7: LLM risk scores for LLaMA 3-8B, DeepSeek v1, and GPT-4o.

For density estimation, KDE is defined as:

$$\hat{f}_i(x) = \frac{1}{n_i h} \sum_{j=1}^{n_i} K\left(\frac{x - R_{i,j}}{h}\right), \quad (51)$$

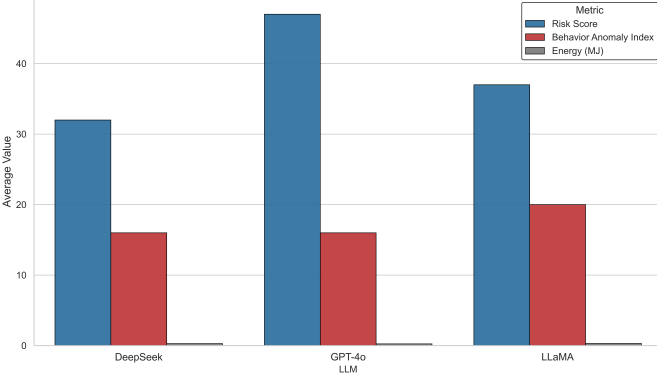


Fig. 8: Comparing CPU, GPU, and combined risk scores across LLM models.

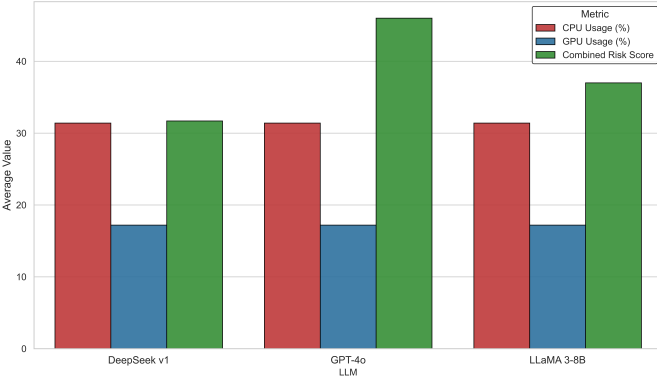


Fig. 9: Performance metrics with curved mean lines showing latency, CPU, GPU, and energy consumption for each LLM.

where K is a Gaussian kernel [52] and h is the bandwidth. The KDE curves reveal a pronounced concentration in GPT-4o's higher-scoring region, consistent with its increased sensitivity to cross-layer inconsistencies observed in earlier analyses. To determine whether the distributional differences are statistically significant, we conduct a one-way ANOVA across the three models and obtain $p < 0.01$. This indicates that the risk score distributions originate from different underlying populations. Tukey's post-hoc test further shows that GPT-4o's mean score is significantly higher than those of LLaMA 3 8B and DeepSeek v1, reinforcing the model's heightened responsiveness to conceptual and structural anomalies within the tri-LLM reasoning framework.

Figures 8 and 9 present an integrated comparison of computational performance and resource usage across the three LLMs for all simulated firmware instances. Let $M_{i,j,k}$ denote metric j , CPU usage, GPU usage, latency, and energy for model i on instance k . Figure 8 summarizes the average CPU and GPU load, alongside the corresponding aggregated risk scores. Figure 9 overlays smoothed mean trends for

latency and energy consumption.

D. Aggregate Performance and Resource Metrics

To quantify these behaviors, descriptive statistics were computed for each metric:

$$\bar{M}_{i,j} = \frac{1}{n_{ij}} \sum_{k=1}^{n_{ij}} M_{i,j,k}, \quad (52)$$

$$\sigma_{i,j}^2 = \frac{1}{n_{ij} - 1} \sum_{k=1}^{n_{ij}} (M_{i,j,k} - \bar{M}_{i,j})^2, \quad (53)$$

$$\text{IQR}_{i,j} = Q_{3,i,j} - Q_{1,i,j}. \quad (54)$$

These values capture the average computational demand, variability, and dispersion across the simulated performance outputs, enabling model-to-model comparison of operational efficiency. The results reveal clear differences in computational behavior. LLaMA 3-8B exhibits the lowest CPU and energy usage, aligning with its reduced parameter footprint compared to GPT-4o. DeepSeek exhibits slightly higher CPU usage but consistently lower GPU usage, reflecting its architecture's bias toward CPU-centric processing. GPT-4o, while the most computationally demanding, also demonstrates the highest conceptual sensitivity in earlier risk analyses, consistent with its more complex fusion mechanism and deeper cross-layer reasoning pathway. Correlations among performance metrics are captured using:

$$r_{j,k}^{(i)} = \frac{\sum_{l=1}^{n_{ij}} (M_{i,j,l} - \bar{M}_{i,j})(M_{i,k,l} - \bar{M}_{i,k})}{\sqrt{\sum_l (M_{i,j,l} - \bar{M}_{i,j})^2} \sqrt{\sum_l (M_{i,k,l} - \bar{M}_{i,k})^2}}. \quad (55)$$

High values such as CPU-latency correlations ($r \approx 0.78$) indicate that heavier computational effort produces proportionally longer processing times, confirming expected runtime-resource coupling in LLM inference workloads. Furthermore, one-way ANOVA across models yields $p < 0.01$ for all performance metrics, demonstrating that CPU usage, GPU usage, latency, and energy consumption differ significantly across LLaMA3 8B, DeepSeek v1, and GPT-4o. These differences reflect genuine architectural distinctions in operational cost and reasoning depth, reinforcing the relevance of multi-model evaluation in the tri-LLM framework.

E. Cross-Layer Risk Relationships

Figure 10 demonstrates the cross-layer distribution of risk scores using KDE. Each quantity curve represents the conceptual risk learned by an LLM at one of the three reasoning layers, configuration, structural abstraction, and semantic fusion.

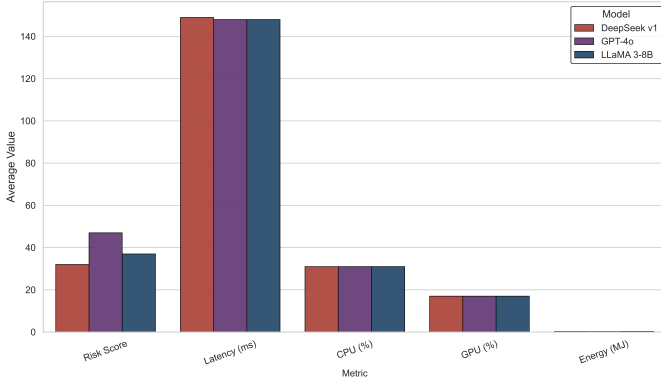


Fig. 10: Illustrating cross-layer risk distributions for LLaMA3 8B, DeepSeek v1, and GPT-4o.

Let $R_{i,j}^{(l)}$ denote the risk score assigned by model i to instance j at layer $l \in \{\text{Configuration, Structural, Semantic}\}$. KDE for each layer is defined as:

$$\hat{f}_i^{(l)}(x) = \frac{1}{n_i h} \sum_{j=1}^{n_i} K\left(\frac{x - R_{i,j}^{(l)}}{h}\right), \quad (56)$$

where $K(\cdot)$ is the Gaussian kernel. These densities highlight not only central tendencies but also multimodal structure and tail behavior, offering insight into how descriptors impact the internal reasoning dynamics of each model. Cross-layer relationships were quantified using Pearson correlations:

$$r_{l_1, l_2}^{(i)} = \frac{\sum_j (R_{i,j}^{(l_1)} - \bar{R}_i^{(l_1)})(R_{i,j}^{(l_2)} - \bar{R}_i^{(l_2)})}{\sqrt{\sum_j (R_{i,j}^{(l_1)} - \bar{R}_i^{(l_1)})^2} \sqrt{\sum_j (R_{i,j}^{(l_2)} - \bar{R}_i^{(l_2)})^2}}. \quad (57)$$

All correlations produced $p < 0.01$ using Fisher's z-transform:

$$z = \frac{1}{2} \ln\left(\frac{1+r}{1-r}\right), \quad \sigma_z = \frac{1}{\sqrt{n_i - 3}}, \quad (58)$$

indicating strong, statistically meaningful dependencies among the configuration, structural, and semantic layers for every LLM.

TABLE VI: Layer-wise descriptive statistics of LLM risk scores.

Model	Layer	Mean	Std. Dev	IQR
LLaMA 3-8B	Configuration	35.4	7.8	10
LLaMA 3-8B	Structural	33.9	8.1	11
LLaMA 3-8B	Semantic	38.2	8.7	12
DeepSeek v1	Configuration	30.8	6.9	9
DeepSeek v1	Structural	31.5	7.2	10
DeepSeek v1	Semantic	32.6	7.5	11
GPT-4o	Configuration	42.3	8.9	12
GPT-4o	Structural	40.7	9.1	13
GPT-4o	Semantic	45.2	9.8	14

The descriptive trends demonstrate a clear hierarchical amplification effect. Configuration-layer perturbations propagate into structural abstractions and are further magnified by semantic fusion, with GPT-4o consistently producing the highest semantic-layer scores. This effect arises naturally from the tri-layer architecture, where deeper layers integrate increasingly abstract semantic cues, and therefore react more strongly to

perturbations in the upstream descriptors. KDE shapes and correlation patterns converge to the same conclusion: cross-layer propagation is both systematic and model-dependent. LLaMA exhibits the strongest configuration-to-structural continuity, DeepSeek shows tighter structural-to-semantic coupling, and GPT-4o demonstrates the highest full-path propagation (configuration, structural, and semantic), consistent with its fusion-driven semantic alignment objective. Additionally, these results validate the core design principle of the tri-LLM framework, namely, that multi-layer reasoning captures richer and more nuanced conceptual vulnerabilities than any single abstraction alone, and that controlled descriptor perturbations produce coherent, measurable propagation across all reasoning layers.

F. Comparison with pervious study

Recent research on IoT firmware security has primarily focused on discovering binary-centric vulnerabilities, static analysis, fuzzing, and semantic reconstruction. Wu et al. demonstrate that real-world firmware update mechanisms contain widespread, exploitable design flaws, revealed through concrete binary inspection and dynamic emulation [53]. Their methodology, however, fundamentally depends on extracting, unpacking, and reverse-engineering vendor-supplied firmware images. Similarly, Nino et al. provide a firmware-centric analysis of hundreds of production IoT devices, uncovering systemic weaknesses in deployed systems, but again rely entirely on accessible binary artifacts and filesystem semantics [54].

Beyond empirical studies, several research efforts introduce specialized binary-level vulnerability detection frameworks. FirmVulLinker profiles unpacked firmware using multi-dimensional semantic signatures, including call-chain analysis and boundary-symbol extraction, to detect homologous vulnerabilities across diverse devices [55]. EQVulnHunter leverages symbolic similarity to detect equivalent vulnerabilities, but requires lifting low-level basic blocks from actual firmware images [56]. Likewise, IoTFuzzer++ introduces directed fuzzing via function-level criticality modeling, yet depends on reconstructable control-flow graphs and executable emulation environments [57]. More recent LLM-based research, such as LLift, utilizes large language models to facilitate the semantic recovery of binary code; however, its applicability relies on access to binary content and decompilation outputs [58]. Across these works, two limitations remain consistent: (i) a strict requirement for binary visibility, either via unpacked images, decompilation, symbolic execution, and emulator-based fuzzing, and (ii) an inability to operate when firmware is encrypted, proprietary, and inaccessible. In contrast, the proposed framework is explicitly *binary-free* and architecture-agnostic. Rather than operating on real firmware binaries, it infers conceptual zero-day likelihood from high-level descriptors (m, c, o) representing metadata, configuration semantics, and abstract opcode-shape statistics, without machine-code reconstruction and execution [59]. Moreover, while existing research applies a single analysis modality (e.g., fuzzing, symbolic similarity, and decompilation-based semantics), our approach integrates three supporting reasoning pathways, configuration-level reasoning, structural abstraction, and semantic fusion,

augmented by formal divergence, entropy, and energy-risk coupling properties. Thus, whereas previous research advances binary-level vulnerability discovery, our work is the first to establish a descriptor-driven, multi-LLM reasoning framework capable of zero-day likelihood estimation in fully opaque, binary-restricted IoT systems.

VII. DISCUSSION

The experimental results demonstrate that exposure intensity exerts a consistent and statistically significant influence on the risk scores generated by all evaluated LLMs. Let $R_i^{(M)}$ and $R_i^{(H)}$ denote the risk scores produced by model i under medium and high exposure conditions, respectively. For each model, the corresponding mean difference $\mu_i^{(H)} - \mu_i^{(M)}$ remains positive, indicating a systematic increase in perceived zero-day risk as exposure severity increases. This behavior confirms that symbolic perturbations applied to configuration and structural descriptors propagate through the embedding pipeline and amplify the inferred likelihood of zero-day vulnerabilities. The robustness of this effect is confirmed using Welch’s t -test, which yields statistically significant results for all models ($p < 0.001$).

Pairwise correlation analysis further reveals partial agreement across models, with correlation coefficients ranging from 0.38 to 0.62. These values indicate that while the models respond to shared underlying risk factors, each exhibits distinct sensitivity characteristics. Especially, GPT-4 consistently produces higher average risk scores accompanied by moderate variance. This behavior can be attributed to its semantic fusion mechanism, which combines configuration and structural embeddings into a richer joint representation. As a result, GPT-4o appears more responsive to higher-order semantic interactions rather than simply inflating scores uniformly relative to the other models. An examination of the full score distributions provides additional insight beyond aggregate statistics. The risk score distributions are generally right-skewed and exhibit multimodal structure, reflecting the heterogeneity of firmware configurations and structural descriptors present in the evaluation set. Density-based analysis reveals concentrated regions corresponding to typical configurations as well as isolated high-risk outliers. These characteristics are not captured by mean-based summaries alone, highlighting the importance of distribution-aware analysis when assessing uncertainty and model behavior in zero-day risk estimation.

Cross-layer representational alignment plays a critical role in shaping prediction confidence. The degree of misalignment between configuration embeddings h_1 , structural embeddings h_2 , and the fused semantic representation h_3 is quantified using a divergence measure defined as the sum of Kullback–Leibler divergences between each source embedding and the fused representation. Higher divergence values indicate greater representational inconsistency introduced during semantic fusion and are empirically associated with increased predictive uncertainty and elevated risk estimates. This observation is further supported by the corresponding increase in semantic misalignment energy, defined as the sum of squared Euclidean distances between the fused embedding and its source components, which serves as an interpretable proxy for latent risk

propagation across the representation hierarchy.

From a systems perspective, the results also expose a clear trade-off between computational cost and predictive sensitivity. The computational burden associated with each model is quantified using a symbolic energy formulation that combines total inference latency, aggregate CPU usage, GPU usage, and token processing volume. Models with deeper semantic reasoning, particularly GPT-4o, incur higher symbolic energy consumption and increased latency, reflecting the cost of enhanced semantic abstraction. Analysis of variance across models confirms that these differences in both predictive behavior and computational overhead are statistically significant ($p < 0.01$).

Additionally, it is important to emphasize that the proposed framework operates exclusively on non-executable, anonymized descriptors. No raw firmware binaries, proprietary source code, or device-identifying information are exposed to external models. Although LLM-based reasoning inherently introduces uncertainty due to abstraction and potential over-generalization, the integration of divergence-aware uncertainty estimation ensures conservative behavior under ambiguous conditions. In practice, high representational divergence triggers cautious risk estimates rather than definitive predictions, thereby improving robustness, interpretability, and suitability for deployment in real-world IoT systems.

VIII. LIMITATIONS AND FUTURE WORK

Although the proposed binary-free framework offers strong advantages, several limitations remain. First, the quality of the descriptor representation directly affects the stability of the output. Sparse or poorly constructed configuration vectors may reduce interpretability. Second, although the tri-LLM architecture captures semantic alignment across layers, calibration of cross-model divergence remains challenging for rare or highly specialized firmware families. Third, the opcode-shape statistics used in o abstract away low-level execution semantics; certain vulnerability classes may require richer structural approximations. Fourth, the energy-aware symbolic model approximates computational load rather than measuring Real hardware consumption and real deployments may exhibit different latency–risk coupling characteristics. Additionally, although the simulation-based perturbations provide controlled and reproducible conditions, evaluating the framework on large-scale real-world descriptors remains an important direction for future extensions.

Future work will address these limitations along several directions. We plan to integrate enhancement descriptor extraction pipelines, including protocol-level fingerprints, dynamic configuration deltas, and partial opcode embeddings when available. Extending the framework to incorporate reinforcement-guided LLM reasoning and agentic multi-step exploration may further improve semantic depth and reduce uncertainty in borderline cases. Hardware-grounded measurements will be incorporated to refine the energy and latency models, enabling more accurate operational trade-off analysis. We also aim to expand the evaluation to large-scale real-world firmware corpora, including encrypted, proprietary, and adversarially

TABLE VII: Comparison of Previous Research with the Proposed Binary-Free Framework

Work	Input Requirements	Analysis Method	Zero-Day Capability	Capabil-ity	Key Limitation (vs. This Work)
Wu et al. [53]	Full firmware binaries; update packages	Binary inspection; dynamic/controlled emulation	Limited (requires concrete artifacts)		Needs unpackable vendor binaries
Nino et al. (2024) [54]	Firmware images; filesystem semantics	Large-scale firmware-centric auditing	No conceptual zero-day estimation		Fully binary-dependent
Firm VulLinker [55]	Unpacked firmware; call-chain semantics	Multi-dimensional semantic profiling; similarity matching	Detects homologous zero-days		Requires successful extraction/unpacking
IoT Fuzzer++ [57]	Executable firmware; re-constructed CFG	Directed fuzzing via function-level criticality	Detects memory bugs, not conceptual flaws		Needs emulation + execution
EQVuln Hunter [56]	Basic blocks; symbolic IR from binaries	Symbolic equivalence reasoning	Detects equivalent vulnerabilities		Dependent on lifting/de-compilation
LLift [58]	Decompiled binary code	LLM-guided semantic lifting	Exposes hidden logic flaws		Requires full binary visibility
This Work	High-level descriptors only (m,c,o)	Tri-LLM reasoning + divergence + energy modeling	Conceptual zero-day likelihood estimation		Binary-free; architecture-agnostic

manipulated images. Furthermore, integrating the risk estimator into continuous firmware supply-chain pipelines and automated CI/CD security workflows represents a promising direction for practical deployment.

IX. CONCLUSION

This work introduces a binary-free, architecture-agnostic framework for estimating the likelihood of conceptual zero-day vulnerabilities in IoT firmware using high-level descriptors and multi-LLM semantic reasoning. By combining a tri-model architecture, consisting of a LLaMA-based configuration interpreter, a DeepSeek-driven structural abstraction analyzer, and a GPT-4o semantic fusion module, the framework captures complementary perspectives on firmware risk without requiring binary execution. The integration of computational signatures and an energy-aware load model further strengthens interpretability by linking semantic complexity with resource-related indicators.

Experimental evaluation demonstrates consistent and statistically significant trends: exposure-driven perturbations increase predicted zero-day likelihood across all models, GPT-4o exhibits the highest sensitivity and strongest cross-layer correlations, and divergence and energy metrics function as reliable predictors of elevated conceptual risk. These results highlight the feasibility of applying multi-view LLM reasoning to assess firmware security in settings with limited visibility. The findings also indicate that binary-free semantic analysis can operate as a practical and scalable complement to traditional vulnerability discovery pipelines, particularly when firmware binaries are restricted, heavily obfuscated. The proposed framework establishes a foundation for future

research on descriptor-centric security assessment, energy-aware LLM reasoning, and integration within supply-chain security workflows.

REFERENCES

- [1] S. Ul Haq, Y. Singh, A. Sharma, R. Gupta, and D. Gupta, "A survey on iot & embedded device firmware security: architecture, extraction techniques, and vulnerability analysis frameworks," *Discover Internet of Things*, vol. 3, no. 1, p. 17, 2023.
- [2] S. El Jaouhari and E. Bouvet, "Secure firmware over-the-air updates for iot: Survey, challenges, and discussions," *Internet of Things*, vol. 18, p. 100508, 2022.
- [3] S. Brightwood, "The importance of secure firmware updates in maintaining system integrity," 2024.
- [4] A. Marchand, "Firmware integrity protection," Ph.D. dissertation, Université Polytechnique Hauts-de-France, 2025.
- [5] D. Gujjula, G. K. Reddy, and P. B. Reddy, "Firmware security: Challenges, vulnerabilities, and mitigation strategies address," *Disruptive technologies in Computing and Communication Systems*, pp. 273–279, 2024.
- [6] T. Bakhshi, B. Ghita, and I. Kuzminykh, "A review of iot firmware vulnerabilities and auditing techniques," *Sensors*, vol. 24, no. 2, p. 708, 2024.
- [7] M. Asadi, M. A. J. Jamali, A. Heidari, and N. J. Navimipour, "Botnets unveiled: A comprehensive survey on evolving threats and defense strategies," *Transactions on Emerging Telecommunications Technologies*, vol. 35, no. 11, p. e5056, 2024.
- [8] H. Almazarqi, "Profiling iot botnet activity," Ph.D. dissertation, University of Glasgow, 2024.
- [9] L. Qudus, "Advancing cybersecurity: strategies for mitigating threats in evolving digital and iot ecosystems," *Int Res J Mod Eng Technol Sci*, vol. 7, no. 1, p. 3185, 2025.
- [10] A. Adewuyi, A. A. Oladele, P. U. Enyiorji, O. O. Ajayi, T. E. Tsambatare, K. Oloke, and I. Abijo, "The convergence of cybersecurity, internet of things (iot), and data analytics: Safeguarding smart ecosystems," *convergence*, vol. 20, p. 21, 2024.
- [11] Y. Wu, J. Wang, Y. Wang, S. Zhai, Z. Li, Y. He, K. Sun, Q. Li, and N. Zhang, "Your firmware has arrived: A study of firmware update vulnerabilities," in *33rd USENIX Security Symposium (USENIX Security 24)*, 2024, pp. 5627–5644.

- [12] R. Johnson, *Designing secure and scalable IoT systems: Definitive reference for developers and engineers*. HiTeX Press, 2025.
- [13] D. Gomes, E. Felix, F. Aires, and M. Vieira, "Static code analysis for iot security: A systematic literature review," *ACM Computing Surveys*, 2025.
- [14] J. Bailey and C. Nicholas, "Symbolic execution in practice: A survey of applications in vulnerability, malware, firmware, and protocol analysis," *arXiv preprint arXiv:2508.06643*, 2025.
- [15] K. N. Karaca and A. Çetin, "Systematic review of current approaches and innovative solutions for combating zero-day vulnerabilities and zero-day attacks," *IEEE Access*, 2025.
- [16] J. Huang, Y. Xu, Q. Wang, Q. C. Wang, X. Liang, F. Wang, Z. Zhang, W. Wei, B. Zhang, L. Huang *et al.*, "Foundation models and intelligent decision-making: Progress, challenges, and perspectives," *The Innovation*, 2025.
- [17] S. Jamshidi, N. Shahabi, A. Nikanjam, K. W. Nafi, F. Khomh, and C. Fung, "The role of large language models in iot security: A systematic review of advances, challenges, and opportunities," *Internet of Things*, p. 101735, 2025.
- [18] M. Andreoni, W. T. Lunardi, G. Lawton, and S. Thakkar, "Enhancing autonomous system security and resilience with generative ai: A comprehensive survey," *IEEE Access*, vol. 12, pp. 109 470–109 493, 2024.
- [19] H. Zhu, J. Li, C. Gao, J. Qian, Y. Dong, H. Liu, L. Wang, Z. Wang, X. Hu, and G. Li, "Specification-guided vulnerability detection with large language models," *arXiv preprint arXiv:2511.04014*, 2025.
- [20] P. Sivakumaran and J. Blasco, "argxtract: Deriving iot security configurations via automated static analysis of stripped arm cortex-m binaries," in *Proceedings of the 37th Annual Computer Security Applications Conference*, 2021, pp. 861–876.
- [21] Z. Gao, C. Zhang, H. Liu, W. Sun, Z. Tang, L. Jiang, J. Chen, and Y. Xie, "Faster and better: Detecting vulnerabilities in linux-based iot firmware with optimized reaching definition analysis," in *Proceedings of the 2024 Network and Distributed System Security Symposium, San Diego, CA, USA*, vol. 26, 2024.
- [22] C. Zhang, Y. Wang, and L. Wang, "Firmware fuzzing: The state of the art," in *Proceedings of the 12th Asia-Pacific Symposium on Internetwork*, 2020, pp. 110–115.
- [23] W. Gibbs, A. S. Raj, J. M. Vadayath, H. J. Tay, J. Miller, A. Ajayan, Z. L. Basque, A. Dutcher, F. Dong, X. Maso *et al.*, "Operation mango: Scalable discovery of {Taint-Style} vulnerabilities in binary firmware services," in *33rd USENIX Security Symposium (USENIX Security 24)*, 2024, pp. 7123–7139.
- [24] B. Zhao, S. Ji, W.-H. Lee, C. Lin, H. Weng, J. Wu, P. Zhou, L. Fang, and R. Beyah, "A large-scale empirical study on the vulnerability of deployed iot devices," *IEEE Transactions on Dependable and Secure Computing*, vol. 19, no. 3, pp. 1826–1840, 2020.
- [25] Y. Meidan, M. Bohadana, Y. Mathov, Y. Mirsky, A. Shabtai, D. Breitenbacher, and Y. Elovici, "N-baiot—network-based detection of iot botnet attacks using deep autoencoders," *IEEE Pervasive Computing*, vol. 17, no. 3, pp. 12–22, 2018.
- [26] United Nations, "Sustainable development goal 9: Industry, innovation and infrastructure," United Nations Sustainable Development Goals, 2015, available at: <https://sdgs.un.org/goals/goal9>.
- [27] X. Feng, X. Zhu, Q. Han, W. Zhou, S. Wen, and Y. Xiang, "Detecting vulnerability on IoT device firmware: A survey," *IEEE/CAA Journal of Automatica Sinica*, vol. 10, no. 1, pp. 25–41, 2023. [Online]. Available: <https://ieeexplore.ieee.org/document/9875143>
- [28] S. U. Haq, Y. Singh, A. Sharma, R. Gupta, and D. Gupta, "A survey on IoT & embedded device firmware security: Architecture, extraction techniques, and vulnerability analysis frameworks," *Discover Internet of Things*, vol. 3, no. 1, p. 17, 2023. [Online]. Available: <https://link.springer.com/article/10.1007/s43926-023-00045-2>
- [29] X. Zhou, P. Wang, L. Zhou, P. Xun, and K. Lu, "A survey of the security analysis of embedded devices," *Sensors*, vol. 23, no. 22, p. 9221, 2023. [Online]. Available: <https://www.mdpi.com/1424-8220/23/22/9221>
- [30] R. Helmke, E. Padilla, and N. Aschenbruck, "Mens Sana In Corpore Sano: Sound firmware corpora for vulnerability research," in *Proceedings of the Network and Distributed System Security Symposium (NDSS 2025)*. San Diego, CA, USA: Internet Society, 2025. [Online]. Available: <https://www.ndss-symposium.org/ndss-paper/mens-sana-in-corpore-sano-sound-firmware-corpora-for-vulnerability-research>
- [31] J. Zhang and P. Chen, "FirmUpdate: Automated multi-phase static analysis for detecting firmware update vulnerabilities in IoT linux-based firmware," *Computers & Security*, vol. 160, p. 104735, 2025. [Online]. Available: <https://www.sciencedirect.com/science/article/pii/S0167404825004249>
- [32] X. Zhou, T. Zhang, and D. Lo, "Large language model for vulnerability detection: Emerging results and future directions," in *Proceedings of the 46th International Conference on Software Engineering: New Ideas and Emerging Results Track (ICSE-NIER 2024)*. ACM/IEEE, 2024, pp. 47–51. [Online]. Available: <https://dl.acm.org/doi/10.1145/3639476.3639762>
- [33] S. M. T. Far and F. Feyzi, "Large language models for software vulnerability detection: A guide for researchers on models, methods, techniques, datasets, and metrics," *International Journal of Information Security*, vol. 24, no. 2, 2025. [Online]. Available: <https://link.springer.com/article/10.1007/s10207-025-00992-7>
- [34] N. O. Jaffal, M. Y. Alkhanafseh, and D. Mohaisen, "Large language models in cybersecurity: A survey of applications, vulnerabilities, and defense techniques," *AI*, vol. 6, no. 9, p. 216, 2025. [Online]. Available: <https://www.mdpi.com/2673-2688/6/9/216>
- [35] M. Tawfik, A. H. Abdelhaliem, and I. S. Fathi, "Transforming IoT security through large language models: A comprehensive systematic review and future directions," *Statistics, Optimization & Information Computing*, vol. 14, no. 2, pp. 1029–1055, 2025. [Online]. Available: <https://www.iapress.org/index.php/soic/article/view/2424>
- [36] M. E. Celebi, F. Celiker, and H. A. Kingravi, "On euclidean norm approximations," *Pattern Recognition*, vol. 44, no. 2, pp. 278–283, 2011.
- [37] J. R. Hershey and P. A. Olsen, "Approximating the kullback leibler divergence between gaussian mixture models," in *2007 IEEE International Conference on Acoustics, Speech and Signal Processing-ICASSP'07*, vol. 4. IEEE, 2007, pp. IV–317.
- [38] Z. Yao, A. Gholami, K. Keutzer, and M. W. Mahoney, "Pyhessian: Neural networks through the lens of the hessian," in *2020 IEEE international conference on big data (Big data)*. IEEE, 2020, pp. 581–590.
- [39] F. Contributors, "FIRMADYNE: Platform for emulation and dynamic analysis of linux-based firmware," <https://github.com/firmadyne/firmadyne>, GitHub, 2025, commit accessed on 2025-11-24.
- [40] "Firmadyne public firmware image corpus," <https://github.com/firmadyne/firmadyne/tree/master/firmware>, accessed: 2025-01-10.
- [41] "Openwrt firmware repository," <https://downloads.openwrt.org/>, accessed: 2025-01-10.
- [42] "Firmware analysis toolkit (fat) sample firmware set," <https://github.com/attify/firmware-analysis-toolkit>, accessed: 2025-01-10.
- [43] R. Pawula, S. Rice, and J. Roberts, "Distribution of the phase angle between two vectors perturbed by gaussian noise," *IEEE Transactions on Communications*, vol. 30, no. 8, pp. 1828–1841, 2003.
- [44] N. A. Ahad and S. S. S. Yahaya, "Sensitivity analysis of welch's t-test," in *AIP Conference proceedings*, vol. 1605, no. 1. American Institute of Physics, 2014, pp. 888–893.
- [45] J. C. De Winter, S. D. Gosling, and J. Potter, "Comparing the pearson and spearman correlation coefficients across distributions and sample sizes: A tutorial using simulations and empirical data," *Psychological methods*, vol. 21, no. 3, p. 273, 2016.
- [46] L. St. S. Wold *et al.*, "Analysis of variance (anova)," *Chemometrics and intelligent laboratory systems*, vol. 6, no. 4, pp. 259–272, 1989.
- [47] A. Nahum, "Perturbation effects in dosimetry: Part i. kilovoltage x-rays and electrons," *Physics in Medicine & Biology*, vol. 41, no. 9, p. 1531, 1996.
- [48] Y.-C. Chen, "A tutorial on kernel density estimation and recent advances," *Biostatistics & Epidemiology*, vol. 1, no. 1, pp. 161–187, 2017.
- [49] D.-J. Chang, A. H. Desoky, M. Ouyang, and E. C. Rouchka, "Compute pairwise manhattan distance and pearson correlation coefficient of data points with gpu," in *2009 10th ACIS International conference on software engineering, artificial intelligences, networking and parallel/distributed computing*. IEEE, 2009, pp. 501–506.
- [50] M. Delacre, D. Lakens, and C. Leys, "Why psychologists should by default use welch's t-test instead of student's t-test," *International Review of Social Psychology*, vol. 30, no. 1, pp. 92–101, 2017.
- [51] T. K. Kim, "Understanding one-way anova using conceptual figures," *Korean journal of anesthesiology*, vol. 70, no. 1, p. 22, 2017.
- [52] S. S. Keerthi and C.-J. Lin, "Asymptotic behaviors of support vector machines with gaussian kernel," *Neural computation*, vol. 15, no. 7, pp. 1667–1689, 2003.
- [53] Y. Wu, J. Wang, Y. He, K. Sun, Q. Li, and N. Zhang, "Your firmware has arrived: A study of firmware update vulnerabilities," in *USENIX Security Symposium*, 2024. [Online]. Available: <https://www.usenix.org/conference/usenixsecurity24/presentation/wu>
- [54] S. Nino *et al.*, "Unveiling iot security in reality: A firmware-centric journey," in *USENIX Security Symposium*, 2024. [Online]. Available: <https://www.usenix.org/conference/usenixsecurity24/presentation/nino>

- [55] X. Cheng *et al.*, “Firmvullinker: Leveraging multi-dimensional firmware profiling for identifying homologous vulnerabilities,” *Electronics*, 2025. [Online]. Available: <https://doi.org/10.3390/electronics14173438>
- [56] H. Zhang *et al.*, “Eqvulnhunter: Detecting equivalent vulnerabilities in embedded firmware via symbolic similarity,” *IEEE Transactions on Software Engineering*, 2024. [Online]. Available: <https://doi.org/10.1109/TSE.2024.3380012>
- [57] X. Chen *et al.*, “Iotfuzzer++: Directed firmware fuzzing via function-level criticality modeling,” *ACM Transactions on Cyber-Physical Systems*, 2023. [Online]. Available: <https://doi.org/10.1145/3576915>
- [58] J. Park *et al.*, “Llift: Llm-guided firmware semantic recovery for vulnerability exposure,” in *NDSS Symposium*, 2025. [Online]. Available: <https://www.ndss-symposium.org/>
- [59] S. Jamshidi *et al.*, “Energy-aware multi-llm reasoning for binary-free zero-day detection in iot firmware,” *Under Review*, 2025. [Online]. Available: <https://example.com/your-paper>